In vivo detection of Staphylococcus aureus endocarditis by targeting pathogen-specific prothrombin activation

HHS Public Access

Author manuscript

Nat Med. Author manuscript; available in PMC 2012 March 01.

Published in final edited form as:

Nat Med. ; 17(9): 1142–1146. doi:10.1038/nm.2423.

In vivo detection of *Staphylococcus aureus* endocarditis by targeting pathogen-specific prothrombin activation

Peter Panizzi, PhD[1,2,3], **Matthias Nahrendorf, MD, PhD**[1,3], **Jose-Luiz Figueiredo, MD**[1], **Jennifer Panizzi, PhD**[4], **Brett Marinelli**[1], **Yoshi Iwamoto**[1], **Edmund Keliher, PhD**[1], **Ashoka A. Maddur, PhD**[6], **Peter Waterman**[1], **Heather K. Kroh, PhD**[6], **Florian Leuschner, MD**[1], **Elena Aikawa, MD, PhD**[1], **Filip K. Swirski, PhD**[1], **Mikael J. Pittet, PhD**[1], **Tilman M. Hackeng, PhD**[5], **Pablo Fuentes-Prior, PhD**[7], **Olaf Schneewind, MD, PhD**[8], **Paul E. Bock, PhD**[6], and **Ralph Weissleder, MD, PhD**[1,9]

[1] Center for Systems Biology, Massachusetts General Hospital and Harvard Medical School, Simches Research Building, 185 Cambridge St., Boston, MA 02114, USA [2] Department of Pharmacal Sciences, Harrison School of Pharmacy, Auburn University, Auburn, AL 36849 USA [4] Nephrology Division, Massachusetts General Hospital, Charlestown, MA, 02129 USA [5] Department of Biochemistry, Cardiovascular Research Institute Maastricht, University Maastricht, Universiteitssingel 50, 6229 ER Maastricht, The Netherlands [6] Department of Pathology, Vanderbilt University School of Medicine, Nashville, TN, 37232 USA [7] Institut de Recerca, Hospital de la Santa Creu i Sant Pau, Sant Antoni Maria Claret 167, 08025 Barcelona, Spain [8] Department of Microbiology, The University of Chicago, Chicago, IL 60637, USA [9] Department of Systems Biology, Harvard Medical School, Boston, MA 02115, USA

Abstract

Coagulase-positive *Staphylococcus aureus* (*S. aureus*) is the major causal pathogen of acute endocarditis, a rapidly progressing, destructive infection of the heart valves. Bacterial colonization occurs at sites of endothelial damage, where (together with fibrin and platelets) it initiates the formation of abnormal growths known as vegetations. Here we report that an engineered analog of prothrombin detected *S. aureus* in endocarditic vegetations via noninvasive fluorescence or PET imaging. These prothrombin derivatives bound to staphylocoagulase and intercalated into growing bacterial vegetations. We also present evidence for bacterial quorum sensing in the regulation of staphylocoagulase expression by *S. aureus*. Staphylocoagulase expression was limited to the

Corresponding author: Matthias Nahrendorf and Ralph Weissleder Center for Systems Biology, CPZN-5206 Massachusetts General Hospital 185 Cambridge Street Boston, MA 02124 USA Tel: 617-726-8226 Fax: 617-726-5708 mnahrendorf@mgh.harvard.edurweissleder@mgh.harvard.edu.

AUTHOR CONTRIBUTIONS P.P. designed experiments, collected and analyzed the data, and wrote the manuscript. J.L.F. developed the endocarditis model. J.P. conducted the *in situ* hybridization experiments. B.M. acquired the PET-CT data and fused images from different modalities. Y.I. and E.A. performed the histology experiments. E.K. synthesized, characterized and optimized the PET reporter. F.L., F.S., and M.P. labeled leukocytes and analyzed data. P.W. performed optical imaging experiments and analyzed data. P.F.P. modeled the chelator in the PET version of the probe. O.S. made knock out bacteria. P.P., A.A.M., H.K.K., T.H. and P.E.B. designed the imaging probe and performed *in vitro* characterization. M.N. and R.W. designed experiments, supervised the project, developed *in vivo* imaging strategies and systems, reviewed, analyzed and discussed data, and wrote the manuscript. All authors edited the manuscript.

[3]Contributed equally

growing edge of mature vegetations, where it was exposed to the host and co-localized with the imaging probe. When endocarditis was induced with an *S. aureus* strain with genetic deletion of coagulases, survival of mice improved, highlighting the role of staphylocoagulase as a virulence factor.

Keywords

endocarditis; staphylocoagulase; prothrombin; noninvasive imaging; von Willebrand factor binding protein

INTRODUCTION

The majority of life-threatening acute endocarditis cases are caused by coagulase-positive *S. aureus* infections. Due to the high mortality (25-47%), there is an urgent clinical need to diagnose *S. aureus* endocarditis early and reliably[1-5]. However, the clinical diagnosis of endocarditis has remained difficult, and primarily relies on unspecific signs such as the occurrence of a new heart murmur, fever, and the detection of circulating bacteria in blood cultures. In this study, we demonstrate the efficacy of targeted imaging strategies for the specific detection of *S. aureus in vivo*. In so doing, we also provide new insight into the role and molecular topography of staphylocoagulase (SC). Our strategy was to tag prothrombin and track its deposition at infection sites, essentially exploiting *S. aureus'* ability to clot human blood[6] to evade immune clearance. SC binds prothrombin with high affinity (K_D ~ 17–72 pM)[7], activates prothrombin through a conformation change[8], and forms an active SC•prothrombin* complex that has all the fibrinogen-clotting abilities of thrombin, but is impervious to physiologic thrombin inhibitors[7,9]. Here, we determined that SC uses a tethering mechanism to facilitate localization of protease activity to the fibrin-rich vegetations. The systemic application of prothrombin analogs as imaging probes allowed SC to capture the circulating agent via high affinity prothrombin binding.

RESULTS

Localization of SC in vegetations

To determine the expression pattern of SC in a vegetation, we established a mouse model of *S. aureus* endocarditis that featured aortic valve bacterial vegetations (Supplementary Fig. 1 and Fig. 1a-c) resembling those in patients. Our method for imaging SC-dependent prothrombin recruitment to the *S. aureus* vegetation relied on the activation of prothrombin by SC, which simultaneously tethers the SC•(pro)thrombin* complex to fibrin(ogen)-rich vegetations (Fig. 1d). We employed a human prothrombin analog in which the active site was modified by a thrombin inhibitor with a protected thiol group. This prothrombin analog was then reacted with Alexa Fluor 680 dye (AF680-ProT). Injection of AF680-ProT into mice with *S. aureus* endocarditis resulted in its deposition into the vegetation (Fig. 1e,f and Supplementary Fig. 1d,e). This observation was consistent across cohorts infected with different strains of *S. aureus* (Tager 104, Xen29, and Xen8.1), but not in mice infected with coagulase-negative *Staphylococcus epidermidis* or in mice without bacteremia (Fig. 1f).

Although bacteria were present throughout the vegetations, immunoreactive staining for SC and von Willebrand factor binding protein (VWbp), an SC-like prothrombin activator[10], was limited to the periphery (Fig. 1g,h and data not shown, respectively). This pattern was also seen using *in situ* hybridization with anti-sense SC RNA (Fig. 1i and Supplementary Fig. 2). AF680-ProT deposition co-localized with SC production and presence at the interface of the vegetations with the host's circulation (Fig. 1j). Together, these findings imply that the location of SC is governed by its expression site rather than by redistribution following secretion. The topography of SC location and activity at the leading edge of vegetations may be caused by differential expression of SC during vegetation development, since in younger lesions with lower bacterial burden the entire *Staphylococcus* population stained positive for SC (Supplementary Fig. 3a,b).

SC - prothrombin tethering mechanism

To determine the molecular mechanism underlying prothrombin recruitment to the vegetations, we performed *in vitro* native gel binding experiments using either the NH_2-terminal active fragment, SC(1-325), or the full-length SC(1-660) (Fig. 2a for domain organization). On incubation of these SC forms with prothrombin and fibrinogen fragment D (FragD), we found that SC(1-325) and prothrombin bound together (Fig. 2b, lane 4), but lacked the ability to interact with FragD (lane 5). SC(1-660), however, formed an SC•prothrombin•FragD ternary complex (Fig. 2c, lane 5).

The dimeric SC•prothrombin* complex is thought to bind to the central E domain of fibrinogen through interactions with the SC NH_2-terminal domain[11]. It is also believed to simultaneously bind to the D domains through seven 27-amino acid COOH-terminal repeats, present on SC. To understand better how AF680-ProT localizes *in vivo* through the binding of SC to FragD, we subjected mixtures of the two proteins to non-denaturing native-gel electrophoresis. During individual reactions, the SC concentration remained constant, while FragD concentrations were increased. Interestingly, we observed excess FragD only after a 5-fold molar excess over SC, indicating that multiple FragD subunits interact with a single SC molecule (Fig. 2d). It is therefore conceivable that SC, secreted during *S. aureus* infection, interacts with at least four fibrinogen/fibrin molecules per SC molecule to form a mega-protein complex. This would then act to anchor the active SC•prothrombin* complex to the growing vegetation. Since the interaction of the COOH-terminal region of SC is distinct from that of the NH_2-terminal prothrombin binding domains, this mega-complex could also bind one prothrombin per SC, a possibility that is consistent with our results (Fig. 2b, lane 5). Direct evidence for the SC repeat binding to FragD was obtained in an experiment that used a recombinant fragment of SC that contained only the pseudo-repeat and the first SC repeat (PR-R1; Fig. 2a). Fluorescence equilibrium binding experiments showed that a fluorescein labeled analog of PR-R1 (PR-R1[5F]) bound FragD with a K_D 36 ± 8 nM (Fig. 2e).

Non-invasive detection and therapeutic monitoring of *S. aureus* endocarditis

We next investigated the use of AF680-ProT to non-invasively detect *S. aureus* endocarditis. Repetitive blood sampling showed that AF680-ProT had a blood half-life of 79 ± 14 minutes. Using fluorescence molecular tomography fused to X-ray computed tomography

(FMT-CT), we found high local concentrations of AF680-ProT in *S. aureus*-induced vegetations 24 hours after injection of the probe (Fig. 3). Subsequently, we investigated the ability of this approach to detect different *S. aureus* strains by inducing endocarditis using three strains that express SC (Tager 104, Xen29, and Xen8.1). FMT-CT revealed that the increased fluorescence signal originated from the left ventricular outflow tract and the ascending aorta, and encompassed the vegetation in the aortic valve (Fig. 3a-c). The fluorescence concentration in the vegetations was then compared to mice without bacteremia and to mice with *S. epidermidis* challenge (Fig. 3d-f). We found that there was a 20-28-fold higher signal associated with the pathogenic *S. aureus* strains.

To determine the specificity of AF680-ProT, we injected the probe into mice in which femoral artery thrombosis was induced by topical application of $FeCl_3$[12]. No accumulation of AF680-ProT was observed (Supplementary Fig. 4). Next, we induced endocarditis with *S. aureus* strains that were deficient in both coagulases, SC and vWbp[13]. In mice infected with these bacteria, AF680-ProT concentration in vegetations was reduced to background levels (Fig. 4a-c). Interestingly, we found improved survival in these mice (Fig. 4d), suggesting that the coagulases increase the virulence of *S. aureus*. Histology from mice infected with SC and VWbp double knock-out *S. aureus* showed leukocyte infiltration in the vegetations and an absence of the protective fibrin barrier (Supplementary Fig. 3c-f), indicating an impaired ability of bacteria to evade the host defense. In an additional control group, 5 mice were infected with an *S. aureus* strain that only lacked SC; in vivo AF680-ProT concentration was reduced to 14% compared to mice that were infected with isogenic wild type Newman strain bacteria ($P < 0.0001$).

We next tested whether AF680-ProT could monitor antibiotic therapy. FMT-CT imaging 48 hours after infection showed that AF680-ProT was able to quantitate the effects of vancomycin (Supplementary Fig. 5). Termination of therapy resulted in a re-occurrence of the infection and a high risk of mortality, similar to relapse observed in some patients.

PET-CT detection of *S. aureus* endocarditis

To apply the targeting mechanism to clinical *S. aureus* detection, we designed a radiolabeled agent for PET imaging. Here, the prothrombin analog was synthesized by alkylation of the free thiol with a maleimide derivative of a diethylenetriaminepentaacetic acid (DTPA) chelator and then reacted with the PET isotope copper-64 (^{64}Cu). A molecular model indicated that the chelator should have the required flexibility to interact with the metal (Fig. 5a,b). PET-CT (Fig. 5c-f) showed a robust localization of ^{64}Cu-DTPA-ProT signal in vegetations, corroborated by ex vivo autoradiography (Fig. 5g). In mice without bacterial injection, we did not observe accumulation of ^{64}Cu-DTPA-ProT at the site of endothelial trauma (Fig. 5i).

Bioluminescence signal from *luxA-E* expressing *S. aureus* Xen8.1 correlated to ^{64}Cu-DTPA-ProT accumulation (Fig. 5g-k), suggesting that the *in vivo* PET signal reflects bacterial burden. Comparison of PET-CT imaging after injection of ^{64}Cu-DPTA-ProT or ^{18}F-FDG labeled leukocytes, a method that is clinically used to identify inflammatory foci[14], showed a higher target to background ratio for ^{64}Cu-DPTA-ProT (Supplementary Fig. 6). Finally, in

preliminary toxicity experiments we did not observe signs of toxicity or clotting abnormalities (Supplementary Fig. 7).

DISCUSSION

Detection and management of acute endocarditis remains a clinical challenge. We continue to lack a means of visualizing bacteria *in situ*, and therefore currently rely on blood cultures for diagnosis. However, negative blood cultures do not rule out the presence of *S. aureus* in valvular vegetations. Here, we present a molecular imaging strategy capable of detecting small amounts of *S. aureus* in endocarditic vegetations. The approach exploits a mechanism used by *S. aureus* to evade the host immune system; namely SC's ability to clot human plasma[9] locally and seal itself off from surveiling immune cells. Prothrombin analogs engineered with fluorescent or PET beacons allowed us to specifically detect *S. aureus* vegetation formation non-invasively, and to monitor antibiotic therapy in mice with acute endocarditis. Furthermore, we showed that prothrombin localizes to growing vegetations via the bifunctional binding capability of SC, which anchored itself to the vegetation through binding multiple fibrin(ogen) D domains, whilst concurrently snaring circulating prothrombin.

The ability for coagulase-positive *S. aureus* to initiate infection under flow conditions, while simultaneously evading the host immune defense, is a remarkable feat that is poorly understood. Our findings demonstrate that SC plays a greater role in the development of vegetations than was previously appreciated[15-18]. We investigated the COOH-terminal repeat units of SC, and found that SC uses these 27-amino acid repeats to form a ternary complex with FragD and prothrombin. Binding of multiple fibrin(ogen) D domains to a single SC molecule may provide the necessary avidity for SC to withstand the shear stress exerted on a growing vegetation, given that a SC repeat has a K_D of 36 ± 8 nM.

Early in vegetation development, SC was ubiquitously expressed throughout the vegetation. As the vegetation matured, however, SC expression at the core was lost. Chevalier et al. recently demonstrated that SC expression was directly repressed by the quorum sensing-controlled RNAIII, which (via direct binding to SC mRNA) arrests translation and facilitates degradation[19]. Our results are consistent with the notion that quorum sensing is responsible for regulating the SC mRNA signal, which would thus control SC-dependent prothrombin localization in developing vegetations. Improved understanding of the role of SC may provide alternative antibiotic drug targets, for instance disrupting growth of the vegetations and their ability to evade host immunity.

Previously proposed techniques for imaging endocarditis have generally lacked specificity for bacterial infection[14,20-22]. The approach reported here focuses on detection of coagulase-positive *S. aureus*, the deadliest pathogen responsible for the majority of acute endocarditis cases. While further studies are needed to explore translation in large animals and humans, the use of a pathogen-targeting PET tracer in patients would not only facilitate identification of *S. aureus* (*i.e.* from '*in vivo* blood cultures'), but could also inform on the site, the bacterial load, and the activity of the infection and thus guide antibiotic and surgical therapy.

METHODS

Mouse model of endocarditis

The right carotid artery of isoflurane (2% / 2L O_2) anesthetized female C57BL/6 mice (Jackson Laboratories) was isolated, and a 1.4 cm segment of 4-0 suture material (Ethicon, Inc.) was inserted down the right carotid artery into the heart to cause damage to the aortic valve. Proper placement of the suture material was evident as the thread pulsated with heart movement. The suture material was left in place to facilitate sustained damage, and to mimic the presence of foreign material such as central lines, a frequent cause of endocarditis in patients. Mice were allowed to recover for 24 hours, and *S. aureus* (1×10^6 CFUs / 100 μl PBS) was injected via tail vein. We initially verified that the recombinant NH_2-terminal fragment SC(1-325) (accession number AY225090) was able to activate mouse prothrombin. Indeed, we found that the mouse SC(1-325)•prothrombin* complex hydrolyzed the chromogenic substrate, H-D-Phe-Pip-Arg-*p*NA (S2238), at a rate that was equivalent that of mouse thrombin ($k_{cat} = 26 \pm 1\ s^{-1}$). We also found that the supernatants of all *S. aureus* strains were able to clot mouse plasma. These data are essential to verify that the mouse is an appropriate model organism to study SC function and regulation *in vivo*, given that there are considerable species effects (Supplementary Table 1). Endocarditis was evident in >85% of the animals, but the size of the vegetations and the extent of occlusion of the aortic valve varied, potentially correlating with the extent of denuded endothelium caused by the mechanical injury. The MGH Subcommittee on Research Animal Care approved all experiments.

Synthesis of AF680-ProT and ^{64}Cu-DTPA-ProT

Active-site inactivated human prothrombin derivatives were generated as previously described[7], through the use of the thioester peptide chloromethyl ketone, N^{α}-[(acetylthio)acetyl]-D-Phe-Pro-Arg-CH_2Cl. This method is similar to that used for generation of other fluorescent labeled derivates[7,23] or for generation of heavy atom derivates of the SC(1-325)•(pre)thrombin complex[8]. Further details are given in the Supplementary Information.

FMT-CT imaging

On day 2 after suture insertion and 24 hours after induction of bacteremia, FMT-CT imaging was performed to interrogate the AF680-ProT incorporation in vegetations. To this end, mice were injected with 30-45 μg AF680-ProT and imaged 24 hours later using an FMT-2500 LX Quantitative Tomography Imaging System (PerkinElmer). After excitation at 680 nm and measurement of emission at 700 nm, a three-dimensional dataset was reconstructed that contained fluorescence concentration per voxel. FMT imaging was accompanied by hybrid X-ray CT angiography (Inveon PET-CT, Siemens) to visualize anatomy. Image fusion was achieved using Osirix software and fiducial markers on the frame of a dedicated multimodal imaging cassette, as described previously[26]. During CT acquisition, Isovue-370 was infused intravenously at 55 μl/min through a tail vein catheter to enhance vascular structures. The CT reconstruction protocol performed bilinear interpolation, used a Shepp-Logan filter, and scaled pixels to Hounsfield units. The isotropic

spatial resolution for CT was 110 μm, and 1 mm for FMT. Fused data sets were used to place regions of interest in the left ventricular outflow tract.

PET-CT studies

The blood half-life of AF680-ProT (30 μg injected) was determined through repeated retro-orbital blood draws, followed by fluorescence imaging of the samples as well as of non-injected control plasma. To characterize further ^{64}Cu-DTPA-ProT localization, a genetically-engineered *S. aureus* strain that stably expressed bioluminescence at sites of infection was used. In these studies, endocarditis was induced in 12 mice, which were then imaged for the presence of bioluminescence signal using an IVIS Imaging System 100 (Caliper LifeSciences). Animals were subsequently injected with 0.92-1.62 mCi of ^{64}Cu-DTPA-ProT and imaged by PET-CT 12 hours later, with a total corporeal activity averaging at 365 μCi. We used an Inveon small animal PET-CT scanner (Siemens), a high resolution Fourier rebinning algorithm, and a filtered back-projection algorithm to reconstruct three-dimensional images. The PET voxel size was 0.796 × 0.861 × 0.861 mm, for a total of 128 × 128 × 159 voxels. Following the PET-CT imaging, the aortic root was excised and imaged for bioluminescence signal (1 min integration). This was followed by overnight exposure on an autoradiography cassette. Plates were read on a Typhoon™ 9400 Variable Mode Imager (GE Healthcare).

Statistical analysis

The results are expressed as mean ± SEM. Statistical comparisons between groups were evaluated by the Student *t* test. A *p* value of 0.05 was considered statistically significant.

An extended method section is available online in the Supplementary Information.

Supplementary Material

Refer to Web version on PubMed Central for supplementary material.

ACKNOWLEDGEMENTS

The authors would like to thank Y. Fisher-Jeffes for review of the manuscript and C. Vinegoni, Z. Mueller, and J. Sullivan for help with imaging and data analysis. The authors would also like to thank T. Foster for materials and helpful suggestions. This work was funded in part by grants from the National Institute of Health F32-HL094010, K99-HL094533 (P.P.); R01-HL096576, R01-HL095629 (M.N.); R01-EB006432, T32-CA79443, R24-CA92782, P50-CA86355 (R.W.) and R37-HL071544, R01-HL038779 (P.E.B.).

REFERENCES

1. Durack, D. Infective and noninfective endocarditis. In: Hurst, JW.; R., CE.; Sonnenblick, EH.; Wenger, NK., editors. The Heart: Arteries and Veins. Vol. Vol. 63. McGraw-Hill; New York: 2001. p. 1230-1255.
2. Mylonakis E, Calderwood SB. Infective endocarditis in adults. N. Engl. J. Med. 2001; 345:1318–1330. [PubMed: 11794152]
3. Cabell CH, Fowler VG Jr. Repeated echocardiography after the diagnosis of endocarditis: too much of a good thing? Heart. 2004; 90:975–976. [PubMed: 15310673]

4. Lalani T, et al. Analysis of the impact of early surgery on in-hospital mortality of native valve endocarditis: use of propensity score and instrumental variable methods to adjust for treatment-selection bias. Circulation. 121:1005–1013. [PubMed: 20159831]
5. Bayer AS, et al. Diagnosis and management of infective endocarditis and its complications. Circulation. 1998; 98:2936–2948. [PubMed: 9860802]
6. Loeb L. The Influence of certain Bacteria on the Coagulation of the Blood. J. Med. Res. 1903; 10:407–419. [PubMed: 19971581]
7. Panizzi P, et al. Novel fluorescent prothrombin analogs as probes of staphylocoagulase-prothrombin interactions. J. Biol. Chem. 2006; 281:1169–1178. [PubMed: 16230340]
8. Friedrich R, et al. Staphylocoagulase is a prototype for the mechanism of cofactor-induced zymogen activation. Nature. 2003; 425:535–539. [PubMed: 14523451]
9. Panizzi P, et al. Fibrinogen substrate recognition by staphylocoagulase.(pro)thrombin complexes. J. Biol. Chem. 2006; 281:1179–1187. [PubMed: 16230339]
10. Kroh HK, Panizzi P, Bock PE. Von Willebrand factor-binding protein is a hysteretic conformational activator of prothrombin. Proc. Natl. Acad. Sci. U. S. A. 2009; 106:7786–7791. [PubMed: 19416890]
11. Friedrich R, et al. Structural basis for reduced staphylocoagulase-mediated bovine prothrombin activation. J. Biol. Chem. 2006; 281:1188–1195. [PubMed: 16230338]
12. Berny MA, et al. Spatial distribution of factor Xa, thrombin, and fibrin(ogen) on thrombi at venous shear. PLoS One. 2010; 5:e10415. [PubMed: 20454680]
13. Cheng AG, et al. Contribution of Coagulases towards *Staphylococcus aureus* Disease and Protective Immunity. PLoS Pathog. 2010; 6(8)
14. Dumarey N, et al. Imaging infection with 18F-FDG-labeled leukocyte PET/CT: initial experience in 21 patients. J. Nucl. Med. 2006; 47:625–632. [PubMed: 16595496]
15. Phonimdaeng P, O'Reilly M, Nowlan P, Bramley AJ, Foster TJ. The coagulase of *Staphylococcus aureus* 8325-4. Sequence analysis and virulence of site-specific coagulase-deficient mutants. Med. Microbiol. 1990; 4:393–404.
16. Salamah AA. Association of coagulase and/or pigmentation with the virulence of a capsule-lacking Staphylococcus aureus in iron-compromised mice. Microbiologica. 1992; 15:75–78. [PubMed: 1556963]
17. Sawai T, et al. Role of coagulase in a murine model of hematogenous pulmonary infection induced by intravenous injection of *Staphylococcus aureus* enmeshed in agar beads. Infect. Immun. 1997; 65:466–471. [PubMed: 9009298]
18. Baddour LM, Tayidi MM, Walker E, McDevitt D, Foster TJ. Virulence of coagulase-deficient mutants of *Staphylococcus aureus* in experimental endocarditis. J. Med. Microbiol. 1994; 41:259–263. [PubMed: 7932618]
19. Chevalier C, et al. *Staphylococcus aureus* RNAIII binds to two distant regions of coa mRNA to arrest translation and promote mRNA degradation. PLoS pathogens. 6:e1000809. [PubMed: 20300607]
20. Rennen HJ, et al. PET imaging of infection with a HYNIC-conjugated LTB4 antagonist labeled with F-18 via hydrazone formation. Nucl. Med. Biol. 2007; 34:691–695. [PubMed: 17707809]
21. Bleeker-Rovers CP, et al. 99mTc-labeled interleukin 8 for the scintigraphic detection of infection and inflammation: first clinical evaluation. J. Nucl. Med. 2007; 48:337–343. [PubMed: 17332609]
22. Rouzet F, et al. Technetium 99m-Labeled Annexin V Scintigraphy of Platelet Activation in Vegetations of Experimental Endocarditis. Circulation. 2008
23. Bock P. Active-site-selective labeling of blood coagulation proteinases with fluorescence probes by the use of thioester peptide chloromethyl ketones. I. Specificity of thrombin labeling. J. Biol. Chem. 1992; 267:14963–14973. [PubMed: 1634535]
24. Panizzi P, et al. Impaired infarct healing in atherosclerotic mice with Ly-6C(hi) monocytosis. J. Am. Coll. Cardiol. 2010; 55:1629–1638. [PubMed: 20378083]

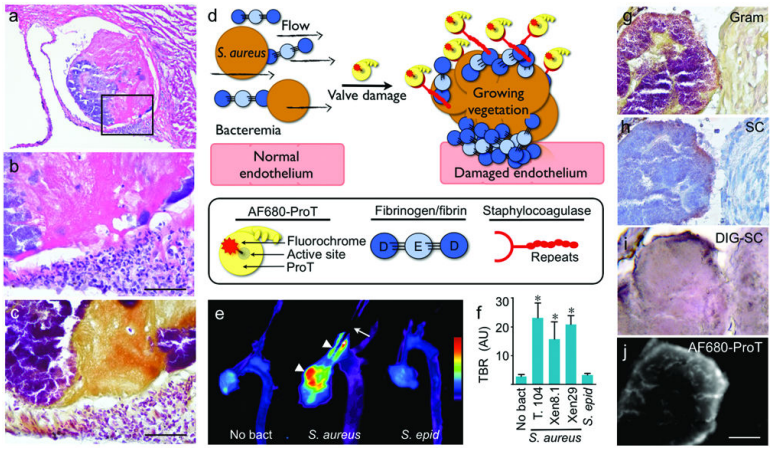

Figure 1. Identification of coagulase-positive endocarditis in a mouse model using a fluorescent prothrombin analog

(**a-d**) Representative *S. aureus* vegetation induced in a murine model of endocarditis. Hematoxylin and Eosin (H&E; **a,b**) and Gram staining (**c,d**) are shown with 400× total magnification in panels (**b**) and (**d**). (**e**) A schematic representation of vegetation formation in *S. aureus* endocarditis including a hypothetical mechanism for probe localization (AF680-ProT, *yellow*) after endothelial trauma and induction of bacteremia. Staphylocoagulase (SC) is shown tethering AF680-ProT to fibrinogen/fibrin via D domain interactions. Fibrinogen (*inset*) has a central E domain flanked by two D domains (*dark blue*). Schematics of AF680-ProT and SC are also shown. (**f-h**) *Ex vivo* fluorescence reflectance imaging (FRI) showed that localization of AF680-ProT is limited to pathogenic *S. aureus*. White light (**f**) and fluorescence images show excised aortas with vegetations (**g**; *arrow heads*) as well as the location of the suture (*arrow*). Quantitation of FRI data is given in panel (**h**) for the controls (either no bacteria or coagulase-negative *S. epidermidis*) and for three *S. aureus* strains. TBR: target to background ratio. * indicates $P < 0.01$. (**i-l**) Microscopic localization of AF680-ProT correlates with SC-positive immunostaining. Gram stain (**i**), SC immunohistochemistry (**j**), *in situ* hybridization against digoxigenin-SC RNA (DIG-SC) (**k**) and fluorescence microscopy (**l**) demonstrate that SC is differentially expressed in growing vegetations and limited to the growing edge. Distance bar equals 50 μm.

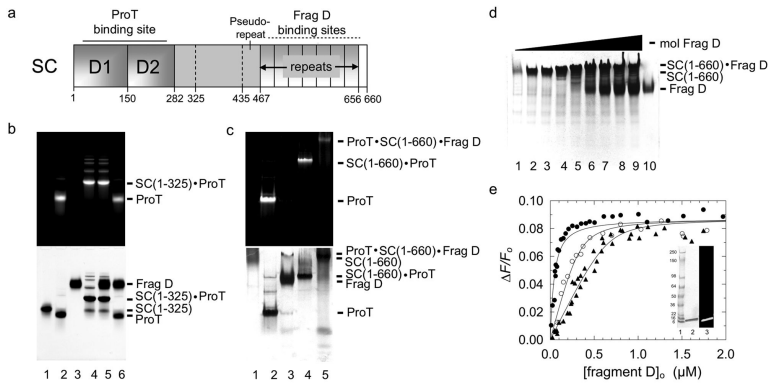

Figure 2. The mechanism underlying fluorescent prothrombin localization during vegetation formation

(**a**) A summary diagram showing that prothrombin binding is limited to the NH_2-terminal SC domains (D1-D2) contained in the SC(1-325) fragment, while SC COOH-terminal repeats bind multiple fibrin(ogen) D domains. (**b**) Fluorescence (*top*) and white light (*bottom*) images of the native gels for the following samples: SC(1-325) (*lane 1*), fluorescent labeled prothrombin (*lane 2*), fragment D (*FragD*) (*lane 3*), labeled prothrombin with 1.1-fold SC(1-325) (*lane 4*), labeled prothrombin with 1.1-fold SC(1-325) and 8-fold molar excess FragD (*lane 5*), labeled prothrombin and FragD (*lane 6*). (**c**) Similar lanes using full-length SC (SC(1-660)) demonstrate the formation of a SC(1-660)•prothrombin•FragD ternary complex (*lane 5*). (**d**) Native gel electrophoresis demonstrating that SC binds multiple FragD domains through COOH-terminal repeats on SC. Mixtures of SC(1-660) with increasing molar ratios of FragD are shown in *lanes 2-9* (1, 2, 4, 5, 6, 7, 8 and 10-fold molar excess of FragD); samples of SC(1-660) and FragD alone were run in lanes 1 and 10, respectively. (**e**) Binding of fragment D to fluorescein-labeled SC pseudorepeat-repeat-1. Titrations of the relative increase in fluorescence ($\Delta F/F_o$) of a 5-(iodoacetamido)fluorescein-labeled Cys residue attached to the COOH-terminus of the SC pseudorepeat-repeat-1 peptide at 20 (filled circle), 430 (open circle), and 855 nM (filled triangle) as a function of the total concentration of fragment D ($[FragD]_o$). *Solid lines* represent the simultaneous least-squares fit of the quadratic binding equation with K_D 36 ± 8 nM, stoichiometric factor 0.77 ± 0.06 mol of fragment D/mol of peptide, and a maximum fluorescence change of 8.7 ± 0.2 %. *Inset:* SDS-PAGE of molecular mass standards in kDa (*lane 1*), protein-stained gel (4 μg, *lane 2*), and fluorescence of the same gel (*lane 3*).

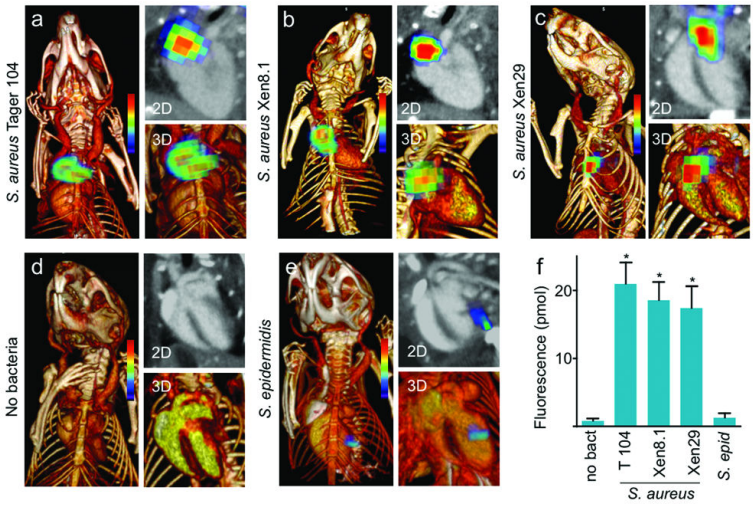

Figure 3. Non-invasive imaging of coagulase-positive *S. aureus* endocarditis via AF680-ProT

Non-invasive fluorescence molecular tomography fused to computed tomography (FMT-CT) of mice infected with three different pathogenic *S. aureus* groups (**a**, Tager 104; **b**, Xen8.1; **c**, Xen29), and two control groups injected with either AF680-ProT but no bacteria (**d**) or with a coagulase-negative *S. epidermidis* strain (**e**). (**f**) Absolute fluorochrome concentration in vegetations quantified by FMT-CT. Data are mean ± SEM, $n = 6$ per group, * $P < 0.01$.

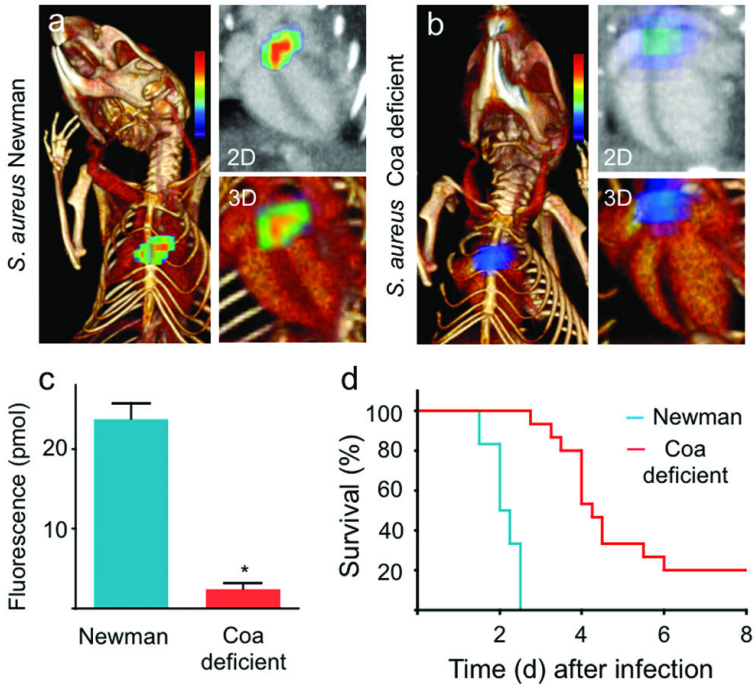

Figure 4. Comparison of AF680-ProT signal in FMT-CT studies of endocarditis in mice infected with *S. aureus* Newman or coagulase-deficient *S. aureus* Newman

Non-invasive fluorescence molecular tomography fused to computed tomography (FMT-CT) of mice infected with (**a**) strain Newman or (**b**) Newman rendered genetically deficient in coagulases SC and VWbp. (**c**) Absolute fluorochrome concentration in vegetations quantified by FMT-CT. Data are mean ± SEM, $n = 6$ per group,* $P < 0.01$ (**d**) Kaplan-Meier curves comparing the survival of mice infected with Newman (*blue line*) or coagulase-deficient Newman (*red line*), n =10-13 per group, median survival 2.1 versus 4.3 days, $P < 0.0001$.

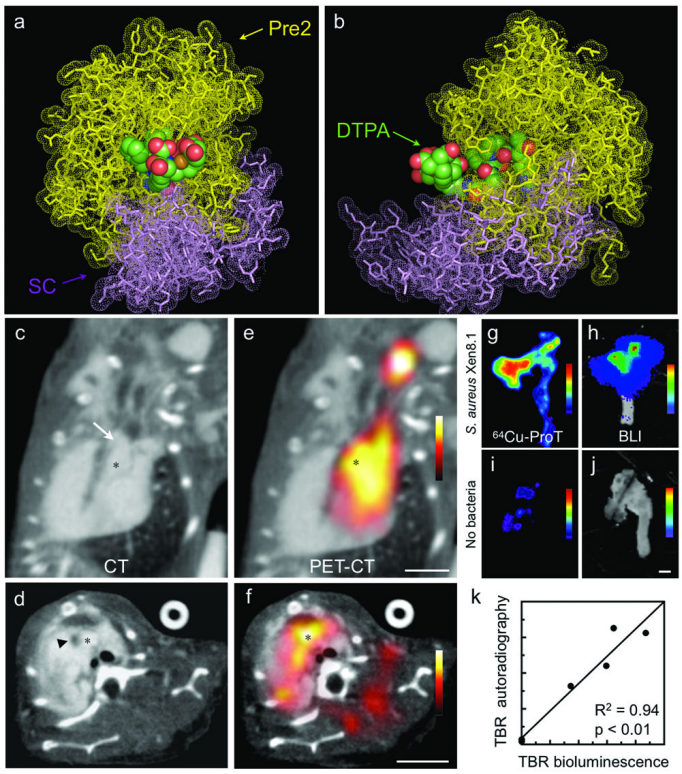

Figure 5. PET-CT imaging of coagulase-positive *S. aureus* endocarditis with Cu^{64}-DTPA-ProT

(**a,b**) Molecular model of Cu^{64}-DTPA in the active site of prethrombin 2 (Pre2; *yellow*) bound to SC (1-325)(*violet*). DTPA atoms are shown as color-coded spheres (carbon, *green*; oxygen, *red*; nitrogen, *blue*; sulfur, *yellow* and copper, *orange*). The two views are related by a 90-degree rotation around the vertical axis. The DTPA moiety was essentially solvent exposed, and moved freely within a region spanned by the 60-, 99- and 148-loops on thrombin. The model indicated that the charged groups on these loops would not affect ^{64}Cu(II) ion coordination, and this was confirmed by the high percentage of ^{64}Cu (89-95% molar ratio) incorporation by the DTPA-ProT recipient. (**c-f**) Representative CT (**c**, long axis; **d**, short axis) and PET-CT images (**e,f**) after injection of Cu^{64}-DTPA-ProT. The inserted suture is denoted by an *arrow*, the aortic valve by an asterisk, and an *arrow head* highlights the vegetation. (**g,j**) Autoradiography and bioluminescence images of excised aortas from a mouse that received Cu^{64}-DTPA-ProT and *S. aureus* Xen8.1 (**g,h**) and from a "no bacteria" control (**i,j**). (**k**) Correlation of probe uptake (autoradiography) with bacterial load in vegetation (bioluminescence).